Macromolecular Bioscience
www.mbs-journal.de

Cy3-Based Nanoviscosity Determination of Mucus: Effect of Mucus Collection Methods and Antibiotics Treatment

Jacqueline Gottwald, Jens Balke, Johannes Stellmacher, Kira van Vorst, Fereshteh Ghazisaeedi, Marcus Fulde, and Ulrike Alexiev*[†]

The integrity of the protective mucus layer as a primary defense against pathogen invasion and microbial leakage into the intestinal epithelium can be compromised by the effects of antibiotics on the commensal microbiome. Changes in mucus integrity directly affect the solvent viscosity in the immediate vicinity of the mucin network, that is, the nanoviscosity, which in turn affects both biochemical reactions and selective transport. To assess mucus nanoviscosity, a reliable readout via the viscosity-dependent fluorescence lifetime of the molecular rotor dye cyanine 3 is established and nanoviscosities from porcine and murine ex vivo mucus are determined. To account for different mucin concentrations due to the removal of digestive residues during mucus collection, the power law dependence of mucin concentration on viscosity is used. The impact of antibiotics combinations (meropenem/vancomycin, gentamycin/ampicillin) on ex vivo intestinal mucus nanoviscosity is presented. The significant increase in viscosity of murine intestinal mucus after treatment suggests an effect of antibiotics on the microbiota that affects mucus integrity. This method will be a useful tool to assess how drugs, directly or indirectly, affect mucus integrity. Additionally, the method can be utilized to analyze the role of mucus nanoviscosity in health and disease, as well as in drug development.

1. Introduction

Cells in the gastrointestinal (GI) and respiratory tract, among others, produce mucus with various functions. Mucus is a natural hydrogel that provides a protective layer as well as a selective barrier. At the macroscale, the mucus layer permits lubrication and protects against dehydration and mechanical insult.[1–3] On the micro- and nanoscale, mucus facilitates the exchange of gases and nutrients while protecting against pathogens.[4] All of these functions require a high dynamic range of the viscoelastic properties of the mucus layer. The details of how mucus can combine all these seemingly contradictory properties are not yet fully understood from a physicochemical perspective.[5] Mucus characterization studies include rats, mice, and more recently, pigs, as the latter's GI tract is most similar to that of humans.[6]

The mucus in the GI tract contains a high degree of water (78–95% in pigs).[6] The most abundant macromolecules in mucus, the mucin proteins, are highly glycosylated and essential for the biochemical and biophysical properties of the mucus.[7] The class of secreted, gel-forming mucins forms the mucus gel lining the luminal epithelial cell surfaces, while the transmembrane mucins are located on the epithelial cell membrane and constitute the glycocalyx.[8,9] One of the most abundant gel-forming mucins throughout the intestinal tract is the mucin 2 protein, forming a large, net-like hydrogel.[6] The secreted mucus in the colon is organized in two layers, of which the inner dense layer is intimately connected to the cell surface and free of bacteria.[10] The outer loose mucus layer extends from the inner layer and harbors the commensal microbiota.[10] Commensal bacteria are expected to use their large number of glycan-degrading enzymes to contribute to the conversion from the thick to the loose mucus layer.[10]

In a healthy state, the nature of the mucus is determined primarily by the mucin network itself, based on its degree of entanglement and cross-linking, and by the solvent properties in the network. Secondary polymers such as DNA and other proteins, as well as lipids present in the inter-mesh solvent naturally influence solvent viscosity.[6]

In the diseased state, the presence of pathogens, cellular debris, and up regulation (or down regulation) of atypical mucins further complicates the situation.[11] Antibiotics are also known to affect the gut microbiota,[12] which in turn can affect mucus integrity through changes in microbiome composition and dy-

J. Gottwald, J. Balke, J. Stellmacher, U. Alexiev[†]
Physics Department
Freie Universität Berlin
Arnimallee 14, 14195 Berlin, Germany
K. van Vorst, F. Ghazisaeedi, M. Fulde
Centre for Infection Medicine
Institute of Microbiology and Epizootics
Freie Universität Berlin
Robert-von-Ostertag-Str. 7, 14163 Berlin, Germany
E-mail: marcus.fulde@fu-berlin.de

The ORCID identification number(s) for the author(s) of this article can be found under https://doi.org/10.1002/mabi.202300437

[†]Deceased

DOI: 10.1002/mabi.202300437

namics. It is, however, less known how this change in the microbiome affects the viscosity of mucus lining the epithelial cells in the GI tract.

Macro- and microrheological techniques, as well as particle tracking rheology, are established techniques for determining the micro- and macroviscosity of mucus as well as its viscoelastic properties from the storage and loss modulus in macrorheology.[13,14]

Recently, ex vivo collection of intestinal mucus from freshly harvested animal tissue and its use as a reliable source for mucus studies aimed at mimicking physiological conditions has been demonstrated.[15] The microviscosity values determined from particle diffusion in native and ex vivo porcine small intestinal mucus are in the same range of 10–19 mPa s.[15] However, sometimes when measuring bulk samples, the properties of the complex mucus network may not reproduce the in vivo behavior, because the measurement method itself may affect the complex mucus network.[16] Microrheology techniques have been established to respond to the requirement of measuring rheology from small volumes of mucus.[14,17] It was also shown that the probe size and the interactions between the probe and mucus must be taken into account in order to select the probe correctly and perform reliable microrheological measurements.[14,18] Furthermore, less attention has been paid to the viscous mucus behavior at the nanoscale, although the transport of small molecules such as nutrients and drugs as well as bacteria not only depends on the microstructural organization of the mucus network but is expected to be significantly influenced by the properties of the solvent on the nanoscale. These nanoscale properties can be sensed by corresponding small nanoscale probes,[19] which do not affect mucus mesh integrity due to their nanometer size. It has been shown that suitable small nanoscale probes are, for example, fluorescent dyes or dyes coupled to soluble proteins.[19,20]

The aim here is to directly determine the nanoviscosity of ex vivo mucus from the cells of the GI tract by establishing the small fluorescent molecular rotor dye cyanine 3 (Cy3) (also called indocarbocyanine (ICC)) with its fluorescence lifetime as a sensor for nanoviscosity.[21] Cy3 belongs to the class of so-called fluorescent molecular rotors that have emerged as novel nanoprobes for dynamic and spatially resolved nanoviscosity sensing,[21–23] based on their ability to undergo intramolecular rotation. In the case of Cy3, the molecular basis of this photophysical property is the twisting motion (*trans–cis* isomerization) of the methine bridge in the excited state of the dye, which has been extensively studied in the past.[24–27] Photoisomerization efficiency depends on solvent viscosity, temperature, and steric restriction.[21,27,28] We recently established a Cy3 dye (ICC) as a fluorescent molecular sensor for membrane nanoviscosity measurements when bound to a sulfated polyglycerol, and extensively characterized the fluorescence behavior of Cy3 as a function of temperature and viscosity.[21] The excited state lifetime of Cy3 (ICC) in aqueous solution is very short ($\tau \approx 0.14$–0.18 ns).[29–31] This is due to the highly efficient bond twisting in the excited state that leads to the nonfluorescent *cis* isomer.[27,32] When bond twisting is hindered, either by friction with solvent molecules (viscosity) (**Figure 1A**) or by steric hindering, for example, through binding to biomolecules, the radiative pathway becomes populated generating fluorescence.[27,28,31,33] To enable mucus viscosity investigations using Cy3, the dye is bound to the mucins via the lectin wheat germ agglutinin (WGA). Lectins are ubiquitous proteins that recognize specific carbohydrate residues of glycoproteins and glycolipids, such as the highly glycosylated mucins. WGA binds specifically to sialic acid and *N*-acetylglucosamine residues of mucin.[34] Figure 1B shows the fluorescence decay curve of Cy3 covalently linked to WGA (WGA-Cy3) whose fluorescence lifetime increases to 1.7 ns in a solution with a viscosity of ≈153 mPa s (lower panel) compared to the fluorescence lifetime of 0.3 ns in aqueous solution (0.9 mPas) (upper panel). Using the Förster–Hoffmann equation,[35] which relates viscosity η to fluorescence lifetime τ with $\log(\tau) \approx \log(\eta)$, the fluorescence lifetime of Cy3 can be translated into viscosity values.[21]

In the present work, we show that WGA-bound Cy3 binds to the sugars of mucins and detects the nanoviscosity of ex vivo porcine and murine mucus. This enables the detection of possible viscosity changes caused by drug treatments, here in this work the treatment with antibiotics. The nanoviscosity method based on the fluorescent molecular rotor Cy3 allows to gain insights into (side)effects of the treatment that affect the mucus integrity.

2. Results and Discussion

2.1. Mucus Autofluorescence

To establish Cy3 as a nanoviscosity sensor for mucus, we first had to determine whether mucus autofluorescence is present and whether this interferes with Cy3 fluorescence. Thus, we measured the autofluorescence of mucus obtained from murine intestinal tissue and commercially available porcine stomach mucus (PSM) (**Figure 2A,B**). The contour plot in Figure 2A demonstrates the steady-state autofluorescence intensity of PSM depending on the excitation and emission wavelength. Autofluorescence shows the most intense fluorescence in the 510–560 nm range, while the fluorescence excitation spectrum shows high intensities below 470 nm. This behavior would agree well with the suggested contribution of collagen to the mucus autofluorescence signal.[36]

The excitation spectrum at the Cy3 excitation wavelength (≈530 nm) shows only residual intensities, while the emission maximum of WGA-Cy3 at ≈560 nm overlaps with the small mucin autofluorescence at this wavelength. Nevertheless, depending on the WGA-Cy3 concentration, the fluorescence contributions from the autofluorescence lifetime curve can influence the Cy3 lifetime signal. Figure 2B shows the autofluorescence lifetime curves from PSM and murine colon mucus in comparison to the fluorescence lifetime curve of WGA-Cy3 in sucrose/water mixtures with viscosities of 0.9 and 153 mPas. As a viscosity sensor, the fluorescence decay curves of WGA-Cy3 cover a wide range of lifetimes.[21] The higher the viscosity, the longer the fluorescence lifetime (Figure 1 and Figure 2B). An increase in WGA-Cy3 fluorescence lifetime measured in samples with unknown mucin concentration could be due to either higher mucus viscosity or simply a larger contribution from mucin autofluorescence since mucin has a longer fluorescence lifetime compared to WGA-Cy3 in aqueous solution (Figure 2B). To use Cy3 as a viscosity sensor, the contribution from autofluorescence to the total fluorescence intensity should be negligible. We estimated

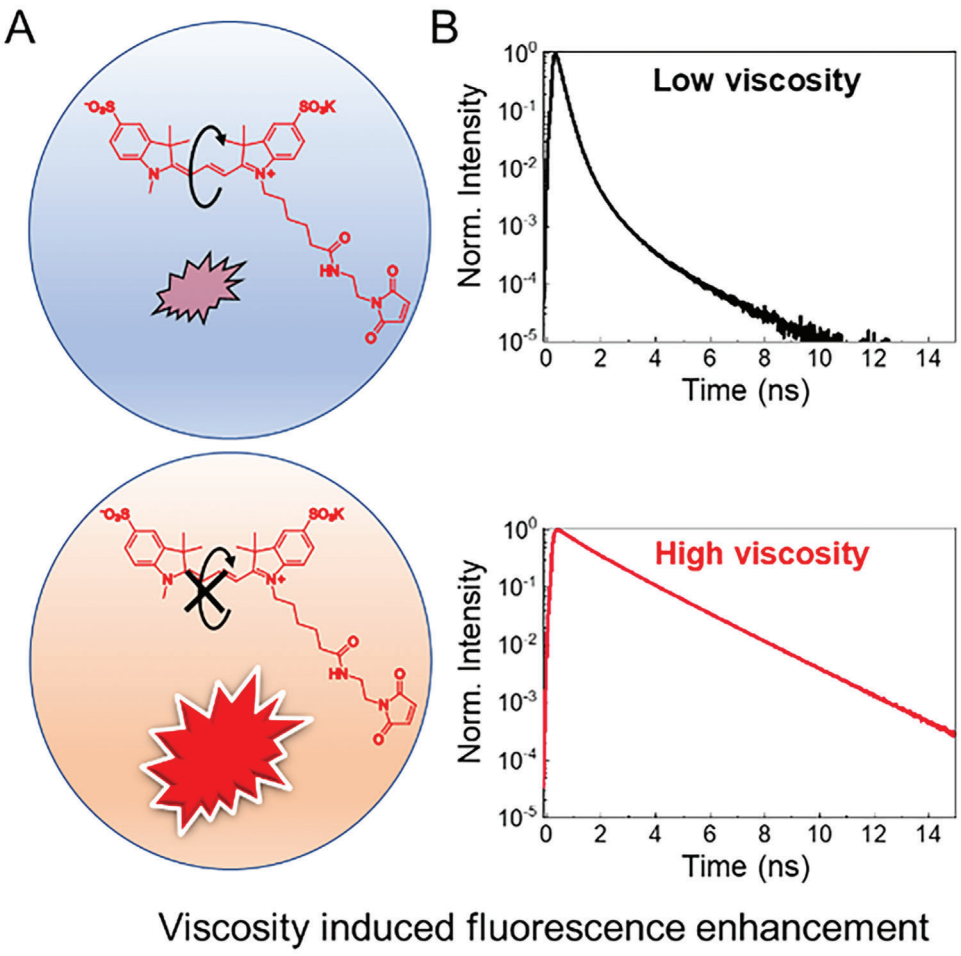

Figure 1. A) Structure of Cy3. The arrow indicates the coordinate for photoisomerization around the C—C double bond in the methine bridge. The upper panel indicates efficient photoisomerization of Cy3 and low fluorescence. The lower panel indicates hindered isomerization due to the presence of a viscous environment and fluorescence enhancement. B) Corresponding fluorescence decay curves showing a fast fluorescence decay (low fluorescence) with a short lifetime (0.3 ns) in aqueous solution and a slow fluorescence decay (high fluorescence) with a long fluorescence lifetime (1.7 ns) in a viscous solution.

that up to 10% autofluorescence would be tolerable for a reliable Cy3 detection.[28] To determine the optimal Cy3 concentration, a mucus sample collected from the murine colon was titrated with increasing concentrations of WGA-Cy3 (Figure 2C). The relative contributions of autofluorescence ($I_{autoflu}$) or WGA-Cy3 ($I_{WGA\text{-}Cy3}$) fluorescence were calculated from the areas under the fluorescence decay curve using $I_{(\text{autoflu or WGA-Cy3})}/(I_{\text{autoflu}}+I_{\text{WGA-Cy3}})$ and plotted as a function of WGA-Cy3 concentration (Figure 2D). At 0.4 μM WGA-Cy3, Cy3 fluorescence is ≈91% and autofluorescence is 9% of total fluorescence in the mucus sample.

2.2. WGA-Cy3 Binding Affinity to Murine Intestinal Mucus

The second requirement for using WGA-Cy3 as a mucus nanoviscosity sensor is that all sensor molecules are bound to mucin. This is the case when the WGA-Cy3 concentration is below the half-maximal binding constant (apparent binding affinity) of WGA-Cy3 to mucin. **Figure 3** shows the binding curve of WGA-Cy3 to the glycosylated mucins in colon mucus. As a lectin, WGA binds primarily to *N*-acetylglucosamine and sialic acid, sugar residues that are common in mucins, via hydrogen bond interactions.[37] The WGA structure and one of its binding pockets to which the mucin sugar moieties bind are presented in Figure 3A. The binding affinity was determined by titrating a diluted murine mucus sample with increasing concentrations of WGA-Cy3 (Figure 3B). The fractional binding saturation values were calculated from the fluorescence lifetime of Cy3 and plotted in a saturation plot (Figure 3C).[31] The lower the WGA-Cy3 concentration, the more complete the binding to the mucus, which is reflected in the longer fluorescence lifetime (Figure 3B). The apparent binding constant in diluted mucus was calculated from the fit to the fractional saturation data (Equation (5)) with K_D = (0.35 ± 0.03) μM.

Calculating back to the original undiluted sample would give an apparent binding constant of K_D = (1.04 ± 0.08) μM. Taking into account the binding affinity and the low autofluorescence background as well as a sufficient Cy3 concentration, we determined 0.3–0.5 μM WGA-Cy3 as the optimal concentration for the following ex vivo mucus nanovicosity experiments.

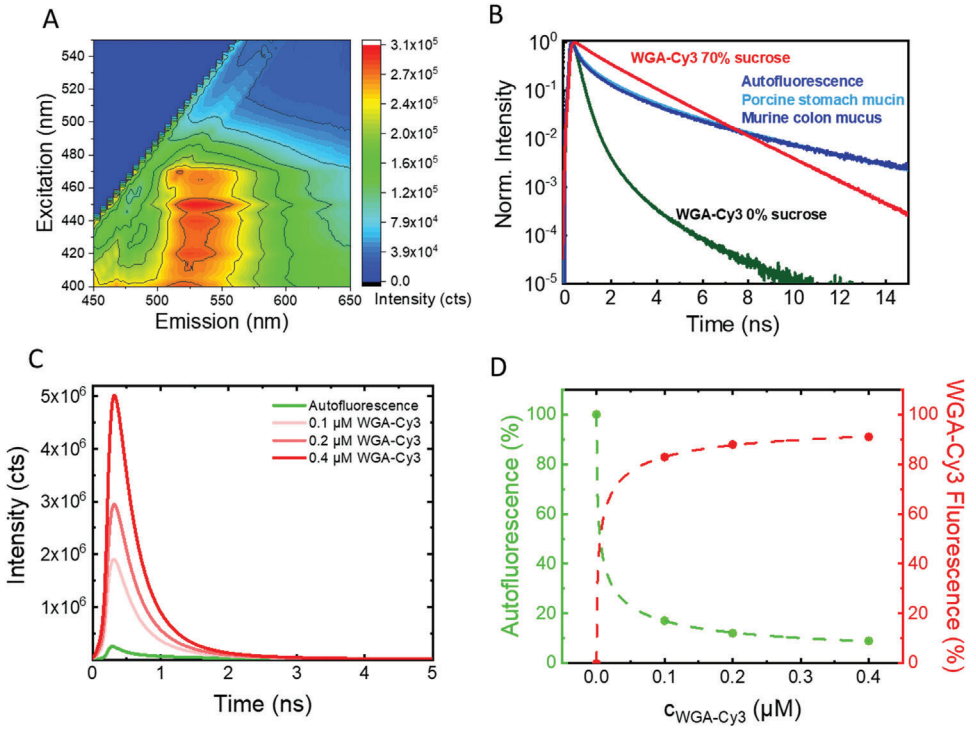

Figure 2. A) Excitation–emission matrix plot of autofluorescence from PSM (2 mg mL^{-1}). B) Fluorescence decay curves of murine intestinal mucus from the colon (dark blue) and PSM (2 mg mL^{-1}) (light blue) compared to the fluorescence decay of WGA-Cy3 in aqueous sucrose mixtures with 0% (black) and 70% (w/w) (red) sucrose. C) Comparison of fluorescence decays of autofluorescence found in murine colon mucus (green) with varying concentrations of WGA-Cy3 in aqueous solution (shades of red). D) Plot of the fraction mucus autofluorescence (green) and the fraction WGA-Cy3 fluorescence (red) as a function of WGA-Cy3 concentration as obtained from (C). Experimental conditions: fluorescence excitation of murine mucus at $\lambda_{ex} = 530$ nm, fluorescence emission at $\lambda_{em} > 545$ nm; PSM: $\lambda^{ex} = 486$ nm and $\lambda^{em} > 515$ nm; $T = 37$ °C.

2.3. Viscosity Calibration

Next, we established the calibration curve (Förster–Hoffmann plot) to calculate the nanoviscosity from the fluorescence lifetime values (**Figure 4**). When using fluorescent molecular rotor dyes to determine viscosity, the viscosity is usually determined from a plot of the fluorescence lifetime of the fluorophore against the bulk viscosity, which is measured, for example, with a rotational viscometer.[21] This is the so-called Förster–Hoffmann plot (Equation (6)) (Figure 4D) and is used as a calibration curve. To investigate the possible influence of WGA-Cy3 binding to mucin on the fluorescence lifetime of Cy3 due to steric hindrance,[27] we used WGA-Cy3 bound to 1 mg mL^{-1} PSM in the respective viscosity solutions. The presence of mucin mimics the natural location of WGA-Cy3 in mucus samples.

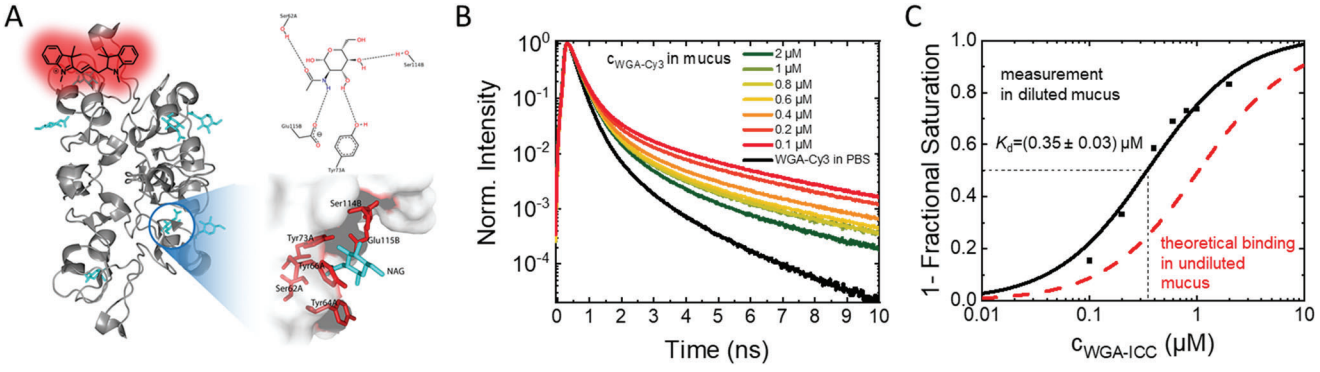

Figure 3. A) Structure of WGA with added Cy3 and its *N*-acetylglucosamine (NAG) binding pocket (pdb 2UVO). B) Fluorescence decays of increasing concentrations of WGA-Cy3 in diluted murine colon mucus (1:3 with phosphate-buffered saline (PBS), pH 7.4). C) Mean fluorescence lifetimes obtained from the decay curves in (B) were used to calculate the fractional binding saturation according to Equation (4), which are plotted in (C). The mucin concentration was kept constant. The fit to a binding equation (Equation (5), black line) is shown. The apparent binding constant is indicated. The red dashed line indicates the binding curve for an undiluted mucus sample. Experimental conditions: $\lambda_{ex} = 530$ nm, $\lambda_{em} > 545$ nm, $T = 37$ °C.

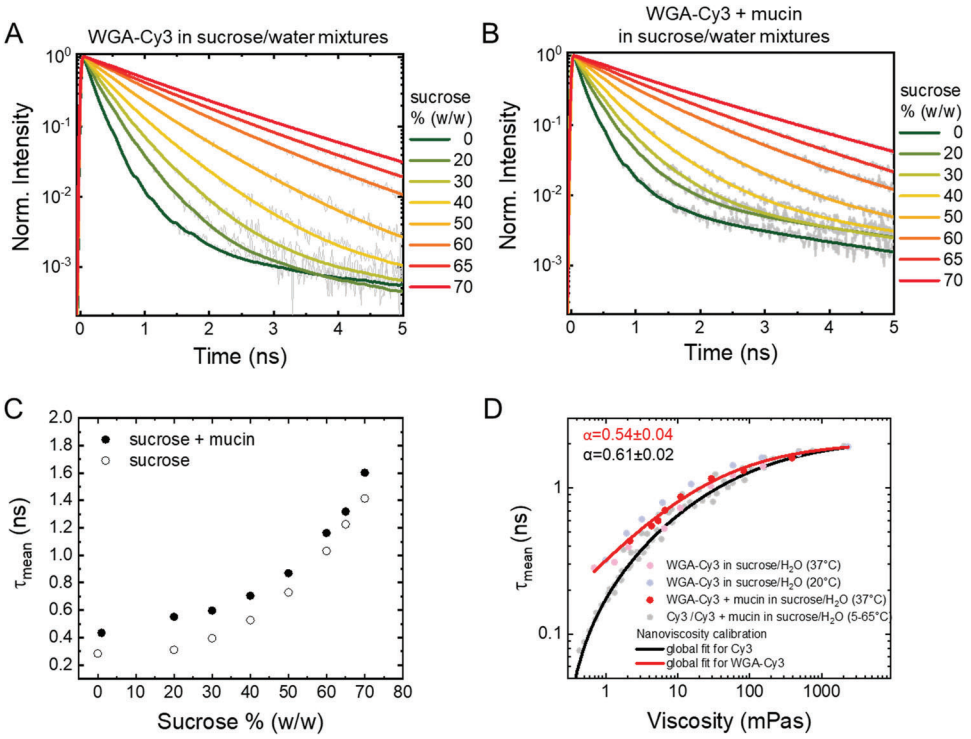

Figure 4. A) Fluorescence decays (gray lines) and multiexponential fits (colored lines) of WGA-Cy3 in different sucrose/buffered water mixtures at 37 °C. B) Fluorescence decays (gray lines) and multiexponential fits (colored lines) of WGA-Cy3 in different sucrose/buffered water mixtures with 1 mg mL^{-1} PSM added at 37 °C. C) Mean fluorescence lifetime (fraction-weighted average lifetime (Equation (2)) of WGA-Cy3 from the fits shown in (A) and (B) are plotted against the sucrose concentration. D) Förster–Hoffmann plots, showing the dependency of the mean fluorescence lifetime (τ_{mean}) on viscosity. A global Förster–Hoffmann fit (Equation (6)) was used to fit the fluorescence lifetime in dependence of bulk viscosity (red and black line). The obtained slopes (α) are indicated. For comparison, the fluorescence lifetime dependence of Cy3 (gray dots) on the bulk viscosity is shown. Experimental conditions for fluorescence lifetime measurements: $\lambda_{ex} = 488$ nm, $\lambda_{em} > 515$ nm, $T = 37$ °C.

As can be seen from the measurements at 0% sucrose (Figure 4A–C), binding to mucin slightly increases the fluorescence lifetime of WGA-Cy3 due to steric hindrance. This results in a slight offset in the viscosity calibration curve compared to Cy3 alone (Figure 4D). Fortunately, the fluorescence lifetime of WGA-Cy3 always responds similarly to the increased viscosity, regardless of whether it is bound to mucins or not, or whether the viscosity increase is caused by sucrose or temperature, all of which are prerequisites for accurate viscosity measurement. The WGA-Cy3 data sets were globally fitted using Equation (6), yielding a slope of $\alpha = 0.54 \pm 0.04$. For the dye Cy3 alone in the presence of mucin, we found a similar slope of $\alpha = 0.61 \pm 0.02$, which agrees very well with earlier data.[21] This slope reflects a very good viscosity sensitivity and points to the 2/3 power viscosity dependence obtained from the Förster–Hoffmann equation for an intermediate viscosity range.[35,38,39]

2.4. Viscosity Determination of Porcine and Murine Intestinal Ex Vivo Mucus

Ex vivo mucus collected from the colon of pigs was measured spectromicroscopically using a fluorescence lifetime imaging microscopy (FLIM) setup to investigate the samples with the lowest possible volume. **Figure 5** shows exemplarily the collected mucus samples (Figure 5A) and the nanoviscosity values at 20 °C (Figure 5B) and 37 °C (Figure 5C). We observed variability between animals, while nanoviscosity values for mucus measurements from a given animal showed less difference. The difference between the two animals was particularly significant at 20 °C with 12 ± 1 and 49 ± 6 mPa s. The difference between the animals was smaller at 37 °C and, with 10 ± 6 and 23 ± 4 mPa s, lies in the range of the viscosity values of ≈10–19 mPa s measured previously with particle tracking.[15]

To compare our measurements with the existing method, we also used the pig colon sample with a 50 nm-sized fluorescent bead for particle diffusivity measurements.[40] The main fraction of freely diffusing particles is ≈70%. A similar value was found in a previous publication in which the intestinal mucus of pigs was studied by particle tracking.[15] The nanoscopic ensemble diffusion constant D amounts to $D = 0.21 \pm 0.01$ μm^2 s^{-1} at 20 °C as calculated from the mean-squared displacements of the bead in the mucus (Figure 5D)[40] The apparent viscosity of $\eta = 41 \pm 2$ mPa s was calculated from the diffusion constant using the Stokes–Einstein equation, $\eta \epsilon = kT/3\pi D\, d$, where k is the Boltzmann constant, T the temperature in Kelvin and d the diameter of the tracer bead ($d = 50$ nm). The comparison of the viscosity values from our tracer measurements with the nanoviscosity measurements from the same sample gives a good agreement taking the interannual variations into account (Figure 5B,E).

Similar variations between animals were found for murine small intestinal and colonic mucus, with nanoviscosity values

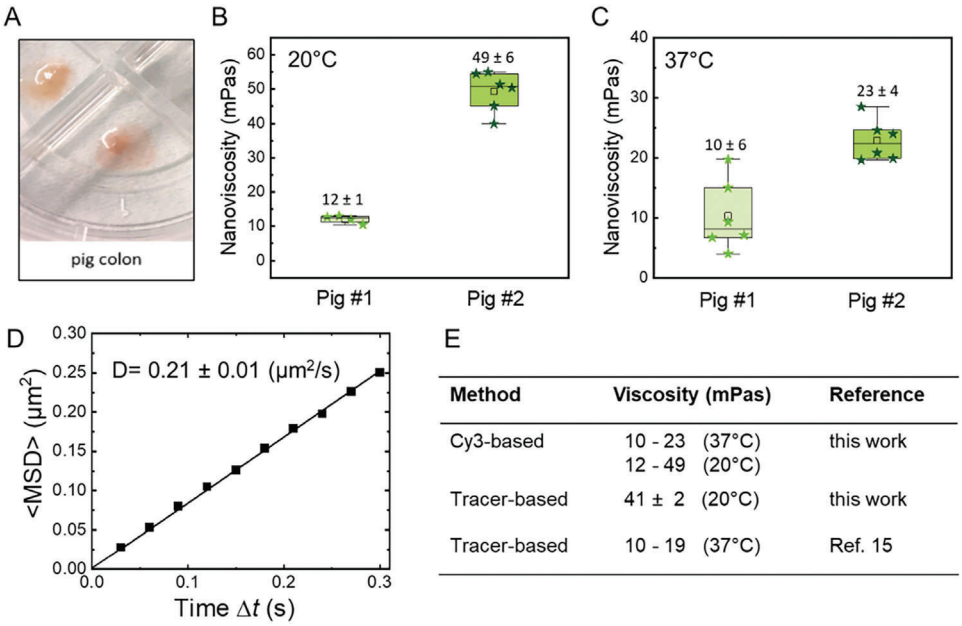

Method	Viscosity (mPas)	Reference
Cy3-based	10 - 23 (37°C) 12 - 49 (20°C)	this work
Tracer-based	41 ± 2 (20°C)	this work
Tracer-based	10 - 19 (37°C)	Ref. 15

Figure 5. A) Small volume sample of washed and scraped pig colon mucus, which was subjected to FLIM measurements. B,C) Nanoviscosity data from mucus obtained from two different animals at 20 °C (B) and 37 °C (C). The mean viscosity values ± SD (in mPa s) with n = 4–6 measurements per animal are indicated. D) Nanoscopic ensemble mean-squared displacements (<MSD>) of fluorescent beads from the mobile fraction of beads as a function of Δt at 20 °C. The calculated diffusion constant with D = <MSD>/4Δt is indicated. E) Comparison of the Cy3-based nanoviscosity method with the existing tracer-based method.

ranging from 16 ± 10 to 172 ± 45 mPa s for colonic mucus depending on the sample and animal and with 32 ± 18 mPa s for small intestinal mucus (**Figure** 6A).

We hypothesize that the washing procedure used to remove digestive residuals before scraping the mucus could influence the measured viscosity values. This would be particularly the case when using smaller animals such as mice. Therefore, we compared washed and unwashed murine colon samples from the same animal (Figure 6B). These results clearly show that using unwashed samples is not an option as the remaining debris from the digestive tract obscures viscosity values and hides possible changes in mucus viscosity (Figure 6B). However, the washing process itself can result in slightly diluted mucus, which can vary depending on the preparation. Therefore, a method is needed that allows evaluation of the effect of treatment on mucus despite possible dilution effects on mucus collection.

2.5. Quantitative Comparison between Different Mucus Samples and Application to Antibiotic Treatment

Given the possible effects of mucus preparation on mucus viscosity presented above, it would be desirable to develop a method that allows comparison of ex vivo mucus samples despite possible dilution effects or natural variations. An example of such a comparative study would be the investigation of the effect of antibiotics on mucus viscosity. Systemic antibiotic treatment is the therapy of choice for serious infections, however, as a side effect,

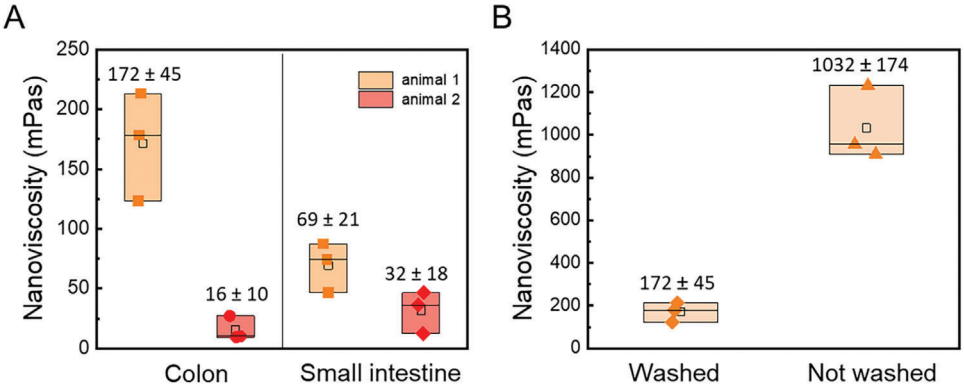

Figure 6. A) Nanoviscosity of scraped ex vivo murine colon mucus and small intestine mucus (20 °C). B) Comparison between washed and unwashed colon mucus samples. The mean viscosity values ± SD (in mPa s) with n = 3 measurements per animal are indicated.

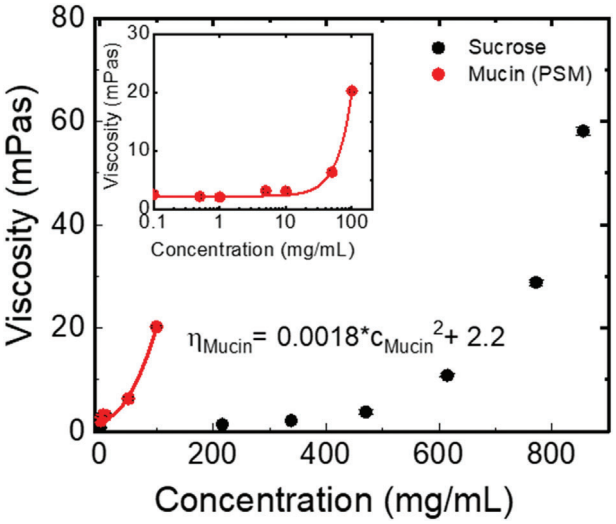

Figure 7. Bulk viscosity dependence of sucrose/water mixtures and mucin/water mixtures on sucrose, respectively, mucin (PSM) concentration. The red solid line represents a fit with a power law function to the mucin data that is indicated in the figure. Inset: Mucin data on a logarithmic *x*-axis.

the systemic use of antibiotic therapy also affects the composition and function of beneficial commensal bacteria/microbiota. Thus, the administration of antibiotics acts as a double-edged sword that perturbs the microbiota and disrupts the homeostasis of the microbiota habitat, that is, of the mucus. We aim here to investigate and compare the physical alterations (viscosity) of intestinal mucus after the administration of systemic antibiotics, mirroring clinical cases. In the present case, we used the antibiotic combinations meropenem/vancomycin and ampicillin/gentamycin, which are commonly used in clinical settings.[41–45]

To account for different mucin concentrations due to the removal of digestive residues during mucus collection, we employed the power law dependence of mucin concentration on viscosity and normalized the viscosity by measuring the mucin concentration using the optical density (OD) at 600 nm. Since the viscosity–concentration correlation is specific for a given polymer[46] we prepared mucin (PSM) at various concentrations and determined the viscosity (**Figure 7**).

The functional correlation can often be described by a power law $\eta = \eta_0 + Ac^b$,[46] where η_0 is the viscosity of the solvent, A, and b are constants and c is the concentration of the polymer, in this case of the biopolymer mucin. The fit for the viscosity dependence on mucin concentration in aqueous solution results in the following fit parameters: $\eta_0 = 2.2 \pm 0.2$ mPa s, $A = (1.8 \pm 6.2) \times 10^{-3}$ mPa s, and $b = 2.0 \pm 0.2$.

In order to apply this power law relationship between mucin concentration and viscosity to normalize the viscosity of ex vivo mucus samples and make the nanoviscosity values comparable, the mucus concentration was determined using the OD at 600 nm. The viscosity data obtained for the different mucus samples should be then normalized by $OD_{600}{}^2$, based on the power law fitting showing that viscosity increases with the square of concentration (Figure 7) and yielding the normalized nanoviscosity value $\eta/OD_{600}{}^2$. We assume that the viscosity decreases when we dilute the mucus to a known extent. However, when we apply the normalization method, the same $\eta/OD_{600}{}^2$ value should be obtained for the diluted and undiluted samples. Thus, to validate this normalization method, we diluted the investigated mucus samples (untreated small intestinal mucus, antibiotics treated small intestinal mucus) by a known factor of 1:1 with PBS and again determined the nanoviscosity and absorbance of the mucus in the diluted samples. The corresponding varying nanoviscosity and OD data are shown in **Figure** 8A,B. We first applied the viscosity normalization to the nanoviscosity values of the untreated sample (Figure 8C). Figure 8C demonstrates that the normalized nanoviscosity value $\eta/OD_{600}{}^2$ indeed is the same, within error, for the diluted (white bar) and undiluted (gray bar) untreated mucus sample. This proves that the $\eta/OD_{600}{}^2$ normalization is characteristic of the given mucus sample and can be used for comparative studies. We also tested the normalization procedures for mucus obtained from a different tissue, pig colon. Normalization shows $\eta/OD_{600}{}^2$ values for undiluted and diluted samples with 7.1 ± 0.7 and 6.7 ± 0.7 mPa s/ $OD_{600}{}^2$, respectively, again with no significant difference.

The normalization procedure now allows a comparison of the different antibiotic treatment effects on small intestinal mucus with the combinations of ampicillin/gentamicin and meropenem/vancomycin (Figure 8D). Treatment with both antibiotic combinations leads to a significant increase in mucus viscosity compared to untreated animals as evidenced by the increased normalized nanoviscosity values (Figure 8D). We can conclude that antibiotic treatment significantly affects the nanoviscosity of small intestinal mucus, approximately leading to a doubling of the normalized nanoviscosity.

The reciprocal interactions between the intestinal mucosal barrier and the gut microbiota play an essential role in maintaining gut homeostasis. Commensal bacteria inhabit the outer mucus layer on mucosal surfaces and utilize their glycans as a prominent energy source.[47–49] Antibiotic treatment induces dysbiosis, which is characterized with altered composition and diversity of the microbiota, functional disturbance of intestinal metabolism, and decreased colonization resistance against pathogens.[50] Subsequently, a shift in the metabolic function of the gut microbiota, accompanied by the overgrowth and invasion of potentially pathogenic bacteria, can trigger inflammatory responses and disrupt tight junctions, leading to a range of complications from diarrhea to enteritis.[51,52] Additionally, thinning of the mucus layer after antibiotic treatment has been reported.[52,53] The latter perhaps could be triggered from a lower total number of bacteria interacting with the mucosal barrier and promoting mucus-production by goblet cells, similar to observations made in germ-free mice.[54] Nevertheless, direct microbiota-mediated effects of antibiotic therapy on the composition, hydrate state, and viscosity of the mucus are still unexplored. Our observations demonstrate an increased mucus nanoviscosity for the two used antibiotics combination, ampicillin/gentamicin and meropenem/vancomycin. Our hypothesis posits that depending on the eliminated bacterial species, decreased taxonomic richness may lead to a general reduction of mucolytic and proteolytic activity of the altered microbiota.[55] In future studies, the inclusion of glycomics and metabolomics investigations will be crucial for unraveling the mechanisms underlying this observation. It is important to acknowledge that the choice of antibi-

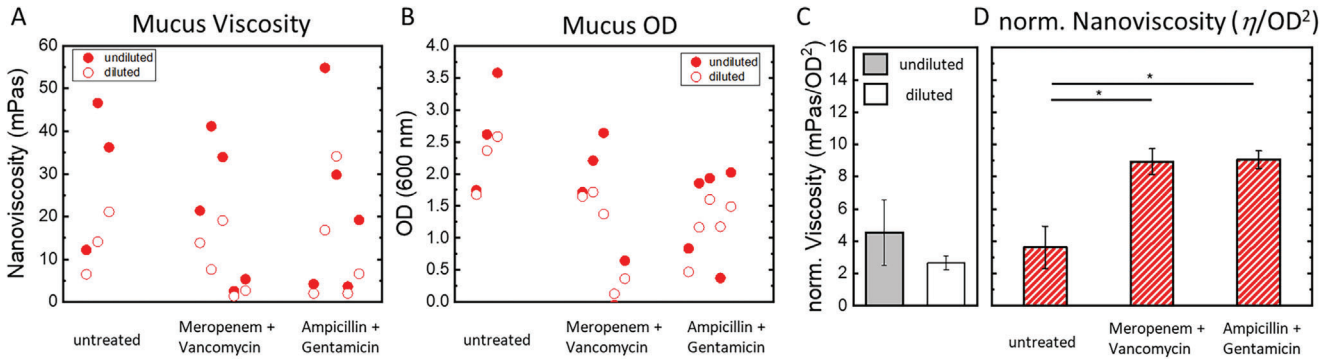

Figure 8. A) Cy3 lifetime-based nanoviscosity values from 0.3 μM WGA-Cy3 in the mucus of the murine small intestine after treatment with two different combinations of antibiotics "Meropenem + Vancomycin" and "Ampicillin + Gentamicin", and from the mucus of an untreated group. B) OD at 600 nm of the mucus samples shown in (A) as a measure of mucin concentration. C) Ratio of nanoviscosity and OD squared (normalized nanoviscosity) for untreated samples. D) Comparison of the normalized nanoviscosity values for the antibiotics-treated groups with the untreated group. "Diluted" samples were diluted 1:1 with PBS before fluorescence decay and absorbance measurements. Experimental conditions: $\lambda_{ex} = 530$ nm, $\lambda_{em} > 545$ nm, $T = 20$ °C. Statistical analysis was performed using a two-way ANOVA and statistical significance was assessed using the Tukey Test (significance level 0.05).

otic class, monotherapy versus combination therapy, dosage, frequency of administration, and treatment duration all play significant roles in shaping the direction and magnitude of microbial perturbations and their mediated effects on the host.[53,56] All of these different factors will be included in future systematic studies. Furthermore, in clinical practice, the administration of probiotics, prebiotics, and fecal microbiota transplantation has been considered during or after a period of antibiotic therapy.[57,58] One main implication from our results is the consideration of combining antibiotic therapies (regardless of the selected antibiotics) with supportive measures to preserve the physical integrity of the mucus layer, for example with the administration of hydrogels or the use of innovative nanodrugs.[59]

3. Conclusion

In summary, a new viscosity sensing modality based on the fluorescent molecular rotor dye Cy3 for mucus viscosity was developed. The lectin-WGA-Cy3 conjugate was shown to bind to the mucin glycans, and conditions were developed to measure mucus nanoviscosity reliably and with high sensitivity using time-resolved fluorescence and the Förster–Hoffmann equation relating fluorescence lifetime to viscosity. Furthermore, we demonstrated that mucus collection, particularly the washing process to remove digestive residues, influences viscosity readings. To account for these unavoidable challenges in the mucus collection process, we established a viscosity normalization based on the squared power law dependence of viscosity on mucin concentration. Analyses of the effects of antibiotics on the small intestine mucus showed an increased mucus nanoviscosity for the two used antibiotics combination, ampicillin/gentamicin and meropenem/vancomycin. We anticipate that the nanoviscosity measurement approach developed here can be broadly applied to all types of mucus from all tissue types. With regard to drug treatments and new drug/mucoadhesive nanoparticle developments, this approach could systematically shed new light on the effects related to mucus integrity.

4. Experimental Section

Collection of Murine and Porcine Mucus Samples: Murine and porcine mucus samples were collected from different intestinal segments in accordance with the principles of the Basel Declaration following the institutional and national guidelines for animal care and use. The protocol was approved by the local state office of occupational health and technical safety "Landesamt für Gesundheit und Soziales, Berlin" (LaGeSo Reg. Nr. T 0284/15 and StN 014/22). Scraped mucus samples were taken from the colon of 6–8 week-old C57BL/6J wild-type mice. In the pig model, samples were obtained from the colon of wild-type German Landrace pigs.

Tissue segments were removed from the body and gently emptied of their contents before being placed in sterile petri dishes. Murine tissues were once flushed with ice-cold sterile cell culture PBS at pH 7.4 (Gibco, Paisley, UK) using a blunt syringe needle. Then intestinal tissues were opened longitudinally using surgery scissors. For porcine tissues, the wash step with ice-cold PBS (2–4 wash steps) was included after the longitudinal cut. Mucus samples were scraped gently using large coverslips. The scraped samples were collected in 2 mL cryotubes (Corning, Reynosa, Mexico), snap-frozen in liquid nitrogen, and stored at −80 °C.

Antibiotics Treatment: Murine mucus samples from 10 juvenile male mice of the same litter were collected (approval G 0167/18). Mice were divided into two groups of 5 and treated with two combinations of antibiotics on the 6th and 7th day after birth with at least 24 h in between treatments. The first group was treated with Ampicillin (orally, 150 mg k^{-1} g) and Gentamicin (orally, 150 mg k^{-1} g), the second group received Meropenem (subcutaneous, 90 mg k^{-1} g) and Vancomycin (orally, 150 mg k^{-1} g). No probiotic was administered after antibiotic treatment. Mucus was obtained from the small intestines and colon. Scraped mucus samples from untreated mice were used as a reference.

Time-Resolved Fluorescence Spectroscopy in FLIM Mode: The fluorescence lifetime curves of Cy3 (sulfo-Cyanine3 maleimide (Lumiprobe, Germany)) and WGA-Cy3 (Biotrend, Germany) in different sucrose/water mixtures, in PSM (Sigma-Aldrich Chemie GmbH, Germany) and in ex vivo mucus were recorded in a home-built confocal time-correlated single photon-counting (TCSPC) based FLIM setup, as previously described,[21,60] to allow the measurement of small samples of 25–50 μL mucus. The setup consisted of an inverted microscope (IX71, Olympus, Shinjuku, Tokio, Japan), a tunable ps-supercontinuum white light laser (SuperK Extreme EXU-3, NKT Photonics, Birkerød, Denmark), a confocal scanning unit (DCS120, Becker & Hickl, Germany), a hybrid PMT detector (HPM-100-40, Becker & Hickl, Germany), and a TCSPC-module (SPC150, Becker & Hickl, Germany). FLIM images were recorded by the SPCM software (Becker & Hickl, Germany) using a 60× objective (water, UPLSAPO60XW, Olympus, Japan), resulting in a total field of view with 300 μm side length. An acousto–optical

tunable filter (SELECT UV–VIS, NKT Photonics, Denmark) was used to select the fluorescence excitation wavelengths from the white light laser beam. The laser repetition rate was set to 19.5 MHz. Cy3 was excited at 530 nm and the fluorescence emission was spectrally selected by a long-pass filter (>545 nm, Chroma, Rockingham, USA). A notch filter (Semrock, USA) removed the residual scattered excitation light. The TCSPC-module sorted the detected fluorescence photons into 1024 time channels with a channel width of 19.97 ps. The instrument response function (IRF) of the system was less than 100 ps (FWHM). To analyze the fluorescence decay traces, the decay histograms from all pixels in the FLIM image were summed up. Subsequently, the fluorescence decay curve was fitted by a multi-exponential model function after deconvolution using a calculated IRF.

$$I\ (t)\ =\ \sum_{i}^{n} \alpha_i\ e^{-t/\tau_i} \tag{1}$$

with n the total number of decay components, α_i the amplitude and τ_i the fluorescence lifetime of the i-th component.[61,62] The fraction-weighted average fluorescence lifetime τ_{mean} was calculated by

$$\tau_{mean}\ =\ \sum_{i}^{n} \beta_i\ \tau_i \tag{2}$$

with β_i being the fractional amplitude (population amplitude) of the i-th component with

$$\beta_i\ =\ \frac{\alpha_i \tau_i}{\sum_i^n \alpha_i \tau_i} \tag{3}$$

In selected cases, the samples were measured in the TCSPC cuvette setup, described in,[62] with an excitation wavelength of 488 nm.

Determination of Apparent Binding Affinity of WGA-Cy3 to Mucin: Half-maximum binding constants (apparent binding affinity, K_D) of WGA-Cy3 to mucins were determined based on changes in Cy3 mean fluorescence lifetime τ_{mean} in the presence of ex-vivo mucus. The fractional saturation of WGA-Cy3 mucin-binding was calculated by:

$$\text{fractional saturation}\ ([BP])\ =\ \left(\frac{\tau_{mean}\ ([BP])\ -\ \tau_{mean,0}}{\tau_{mean,max}\ -\ \tau_{mean,0}}\right) \tag{4}$$

where τ_{mean} is the mean fluorescence lifetime of Cy3 (Equation (2)) at a specific concentration of the binding partner [BP] WGA-Cy3 that binds to mucin. $\tau_{mean,0}$ is the mean fluorescence lifetime of Cy3 in the absence of mucins and $\tau_{mean,max}$ it's lifetime at a theoretical infinite mucin concentration (or at a given mucin concentration with very low WGA-Cy3 concentration) which resulted in fully saturated binding.[31] Thus, the K_D was obtained when plotting 1-fractional saturation over [WGA-Cy3] and the plot was fitted with the Hill-equation:

$$\text{fractional saturation}\ ([BP])\ =\ \frac{S \times [BP]^n}{\left(K_D^n + [BP]^n\right)} \tag{5}$$

where S is the saturation level of the binding process and n is the cooperativity factor (which was 1). Binding experiments were carried out with murine colon mucus with fixed but unknown mucin concentration.

Viscosity Dependence of Cy3 Fluorescence Decay Traces: Cy3 (Lumiprobe, Germany) and WGA-Cy3 (Biotrend, Germany) were investigated by time-resolved fluorescence spectroscopy in sucrose/water mixtures ranging from 0% to 70% (w/w) sucrose. The obtained fluorescence decay traces were fitted by Equation (1) and the mean fluorescence lifetimes were calculated by Equation (2). The viscosity dependence was analyzed as previously described for a Cy3 dye.[21] Briefly, the viscosity values were taken from ref. [63] at the different sucrose concentrations. The mean fluorescence lifetimes as a function of viscosity were evaluated by an extended Förster–Hoffmann equation, which included a temperature-dependent activation energy for dye isomerization:

$$\tau_{mean}\ =\ \left(\frac{1}{C\eta^{\alpha}\ +\ \frac{1}{A_{max}}}\ \times\ e^{-\frac{E_a}{kT}}\ +\ k_f\ +\ k_x\right)^{-1} \tag{6}$$

C is a constant and $1/A_{max}$ indicates that τ does not go to zero at zero viscosity, k_f and k_x are the rate of fluorescence and all other non-radiative rates, respectively, from the excited to the ground state.[21,64]

Diffusivity Measurements: The fluorescence microscopy setup[65] consisted of an inverted wide-field microscope (Olympus IX-71) with a 60× oil immersion objective (PLAPON60xOTIRFM, Olympus) with a numerical aperture of 1.45. Excitation of the samples was achieved with a 25 mW 561 nm laser (MBL III561, CNI Optoelectronics Technology). Fluorescence emission was collected by the same objective and separated from excitation light and possible scattering by a dichroic beam splitter (BS-z488/563/633, Chroma, USA.) and a long pass filter (ET LP 575, Chroma) in the emission path. Emission was detected by a CMOS camera (OrcaFlash V2, Hamamatsu). The recorded movies consisted of 2000 frames with a frame rate of 31 ms/frame and a field of view of 2048 × 2048 pixels with a pixel length of 104 nm that was measured with proper gratings. The identification and calculation of the step length distribution (SLD) and the mean square displacement (MSD) were carried out as described.[40] The sample was scraped mucus from the porcine colon. Mucus (50 µl) was incubated with Cy3-labeled polystyrene beads (PS50-AMS3-1, Nanocs), (1:100 diluted in mucus) for 60 min. Bead diffusion was measured at 20 °C.

To analyze the SLDs the field of view-corrected SLD was used.[40] The MSD of the mobile population was used to calculate the diffusion constant D using

$$\mathrm{D} =< \mathrm{MSD} > /4D\Delta t \tag{7}$$

The Stokes–Einstein equation relates the viscosity η of the mucus to the diffusion coefficient of a particle with diameter d and was used to calculate the viscosity

$$\mathrm{h} = \mathrm{kT}/3\pi Dd \tag{8}$$

Acknowledgements

The protocol was approved by the local state office of occupational health and technical safety "Landesamt für Gesundheit und Soziales, Berlin" (LaGeSo Reg. Nr. T 0284/15 and StN 014/22). Support by the German Research Foundation (DFG, SFB 1449 project ID 431232613 to M.F. and U.A.) was gratefully acknowledged.

Open access funding enabled and organized by Projekt DEAL.

Conflict of Interest

The authors declare no conflict of interest.

Data Availability Statement

The data that support the findings of this study are available from the corresponding author upon reasonable request.

Keywords

antibiotics, antibiotics effect on gastrointestinal (GI) tract, cyanine 3, ex vivo mucus viscosity, fluorescent molecular rotors, mucus nanoviscosity

Received: September 25, 2023
Revised: December 21, 2023
Published online: June 26, 2024

[1] C. Atuma, V. Strugala, A. Allen, L. Holm, *Am. J. Physiol.* **2001**, *280*, 922.
[2] M. E. V. Johansson, H. Sjövall, G. C. Hansson, *Nat. Rev. Gastroenterol. Hepatol.* **2013**, *10*, 352.
[3] C. T. Nordgard, K. I. Draget, *Eur. J. Pharm. Biopharm.* **2015**, *95*, 144.
[4] M. Phillipson, C. Atuma, J. Henriksnas, L. Holm, *Am. J. Physiol.* **2002**, *282*, 211.
[5] C. E. Wagner, M. Krupkin, K. B. Smith-Dupont, C. M. Wu, N. A. Bustos, J. Witten, K. Ribbeck, *Biomacromolecules* **2023**, *24*, 628.
[6] V. Barmpatsalou, I. R. Dubbelboer, A. Rodler, M. Jacobson, E. Karlsson, B. L. Pedersen, C. A. S. Bergstrom, *Eur. J. Pharm. Biopharm.* **2021**, *169*, 156.
[7] D. Ambort, M. E. V. Johansson, J. K. Gustafsson, A. Ermund, G. C. Hansson, *Cold Spring Harbor Perspect. Med.* **2012**, *2*, 014159.
[8] M. Backstrom, D. Ambort, E. Thomsson, M. E. Johansson, G. C. Hansson, *Mol. Biotechnol.* **2013**, *54*, 250.
[9] S. Bafna, S. Kaur, S. K. Batra, *Oncogene* **2010**, *29*, 2893.
[10] M. E. Johansson, J. M. Larsson, G. C. Hansson, *Proc. Natl. Acad. Sci. USA* **2011**, *108*, 4659.
[11] M. A. Hollingsworth, B. J. Swanson, *Nat. Rev. Cancer* **2004**, *4*, 45.
[12] S. R. Modi, J. J. Collins, D. A. Relman, *J. Clin. Invest.* **2014**, *124*, 4212.
[13] F. Del Giudice, M. Tassieri, C. Oelschlaeger, A. Q. Shen, *Macromolecules* **2017**, *50*, 2951.
[14] S. K. Lai, Y. Y. Wang, D. Wirtz, J. Hanes, *Adv. Drug Delivery Rev.* **2009**, *61*, 86.
[15] A. Macierzanka, A. R. Mackie, L. Krupa, *Sci. Rep.* **2019**, *9*, 17516.
[16] L. E. Enjuto, M. R. D. Vincent, M. Maurin, B. Degano, H. Bodiguel, *Sci. Rep.* **2023**, *13*, 7695.
[17] J. Kirch, A. Schneider, B. Abou, A. Hopf, U. F. Schaefer, M. Schneider, C. Schall, C. Wagner, C. M. Lehr, *Proc. Natl. Acad. Sci. USA* **2012**, *109*, 18355.
[18] M. Jory, K. Bellouma, C. Blanc, L. Casanellas, A. Petit, P. Reynaud, C. Vernisse, I. Vachier, A. Bourdin, G. Massiera, *Front. Phys.* **2019**, *7*, 19.
[19] J. Szymanski, A. Patkowski, A. Wilk, P. Garstecki, R. Holyst, *J. Phys. Chem. B* **2006**, *110*, 25593.
[20] J. Szymanski, A. Patkowski, J. Gapinski, A. Wilk, R. Holyst, *J. Phys. Chem. B* **2006**, *110*, 7367.
[21] K. Ober, P. Volz-Rakebrand, J. Stellmacher, R. Brodwolf, K. Licha, R. Haag, U. Alexiev, *Langmuir* **2019**, *35*, 11422.
[22] E. Gatzogiannis, Z. Chen, L. Wei, R. Wombacher, Y. T. Kao, G. Yefremov, V. W. Cornish, W. Min, *Chem. Commun.* **2012**, *48*, 8694.
[23] N. A. Hosny, C. Fitzgerald, C. Tong, M. Kalberer, M. K. Kuimova, F. D. Pope, *Faraday Discuss.* **2013**, *165*, 343.
[24] P. F. Aramendia, R. M. Negri, E. S. Roman, *J. Phys. Chem. B* **1994**, *98*, 3165.
[25] R. Humphry-Baker, M. Graetzel, R. Steiger, *J. Am. Chem. Soc.* **1980**, *102*, 847.
[26] K. Luby-Phelps, S. Mujumdar, R. B. Mujumdar, L. A. Ernst, W. Galbraith, A. S. Waggoner, *Biophys. J.* **1993**, *65*, 236.
[27] E. M. S. Stennett, M. A. Ciuba, S. Lin, M. Levitus, *J. Phys. Chem. Lett.* **2015**, *6*, 1819.
[28] R. Brodwolf, P. Volz-Rakebrand, J. Stellmacher, C. Wolff, M. Unbehauen, R. Haag, M. Schafer-Korting, C. Zoschke, U. Alexiev, *Theranostics* **2020**, *10*, 6322.
[29] A. Boreham, R. Brodwolf, M. Pfaff, T.-Y. Kim, T. Schlieter, L. Mundhenk, A. D. Gruber, D. Gröger, K. Licha, R. Haag, U. Alexiev, *Polym. Adv. Technol.* **2014**, *25*, 1329.
[30] A. Boreham, R. Brodwolf, K. Walker, R. Haag, U. Alexiev, *Molecules* **2016**, *22*, 17.
[31] A. Boreham, J. Pikkemaat, P. Volz, R. Brodwolf, C. Kuehne, K. Licha, R. Haag, J. Dernedde, U. Alexiev, *Molecules* **2015**, *21*, 22.
[32] E. Akesson, V. Sundstrom, T. Gillbro, *Chem. Phys. Lett.* **1985**, *121*, 513.
[33] V. Sundström, T. Gillbro, *J. Phys. Chem.* **1985**, *83*, 2733.
[34] F. Jeffers, C. Fuell, L. E. Tailford, D. A. MacKenzie, R. J. Bongaerts, N. Juge, *Carbohydr. Res.* **2010**, *345*, 1486.
[35] T. Förster, G. Hoffmann, *Z. Phys. Chem.* **1971**, *75*, 63.
[36] Y. C. Wu, P. Xi, J. A. Y. Qu, T. H. Cheung, M. Y. Yu, *Opt. Express* **2004**, *12*, 3218.
[37] M. Monsigny, A. C. Roche, C. Sene, R. Mageтdana, F. Delmotte, *Eur. J. Biochem.* **1980**, *104*, 147.
[38] M. A. Haidekker, E. A. Theodorakis, *J. Biol. Eng.* **2010**, *4*, 11.
[39] C. E. Kung, J. K. Reed, *Biochemistry* **1986**, *25*, 6114.
[40] A. Wolf, P. Volz-Rakebrand, J. Balke, U. Alexiev, *Small* **2023**, *19*, 2206722.
[41] R. Abu Shqara, D. Glikman, S. Jad, H. Rechnitzer, L. Lowenstein, M. F. Wolf, *Am. J. Obstet. Gynecol.* **2023**, *229*, 540.e1.
[42] F. Schneider, A. Gessner, N. El-Najjar, *Antibiotics* **2022**, *11*, 173.
[43] C. M. Sharma, R. P. Agrawal, H. Sharan, B. Kumar, D. Sharma, S. S. Bhatia, *J. Clin. Diagn. Res.* **2013**, *7*, 2511.
[44] Y. Szterenlicht, Y. Steinmetz, Z. Dadon, Y. Wiener-Well, *J. Infect. Chemother.* **2023**, *23*, 1341.
[45] R. Wise, J. P. Ashby, J. M. Andrews, *J. Antimicrob. Chemother.* **1989**, *24*, 233.
[46] A. Ibarz, J. Pagan, R. Miguelsanz, *J. Food Eng.* **1992**, *15*, 63.
[47] J. K. Gustafsson, M. E. V. Johansson, *Nat. Rev. Gastroenterol. Hepatol.* **2022**, *19*, 785.
[48] M. E. V. Johansson, M. Phillipson, J. Petersson, A. Velcich, L. Holm, G. C. Hansson, *Proc. Natl. Acad. Sci. USA* **2008**, *105*, 15064.
[49] A. Schutte, A. Ermund, C. Becker-Pauly, M. E. V. Johansson, A. M. Rodriguez-Pineiro, F. Backhed, S. Muller, D. Lottaz, J. S. Bond, G. C. Hansson, *Proc. Natl. Acad. Sci. USA* **2014**, *111*, 12396.
[50] K. Lange, M. Buerger, A. Stallmach, T. Bruns, *Dig. Dis.* **2016**, *34*, 260.
[51] L. V. McFarland, *Future Microbiol.* **2008**, *3*, 563.
[52] T. Shah, Z. Baloch, Z. Shah, X. M. Cui, X. S. Xia, *Int. J. Mol. Sci.* **2021**, *22*, 6597.
[53] M. Wlodarska, B. Willing, K. M. Keeney, A. Menendez, K. S. Bergstrom, N. Gill, S. L. Russell, B. A. Vallance, B. B. Finlay, *Infect. Immun.* **2011**, *79*, 1536.
[54] J. Petersson, O. Schreiber, G. C. Hansson, S. J. Gendler, A. Velcich, J. O. Lundberg, S. Roos, L. Holm, M. Phillipson, *Am. J. Physiol.* **2011**, *300*, 327.
[55] H. E. Jakobsson, A. M. Rodriguez-Pineiro, A. Schutte, A. Ermund, P. Boysen, M. Bemark, F. Sommer, F. Backhed, G. C. Hansson, M. E. V. Johansson, *EMBO Rep.* **2015**, *16*, 164.
[56] P. Zimmermann, N. Curtis, *J. Infect.* **2019**, *79*, 471.
[57] H. Duan, L. Yu, F. Tian, Q. Zhai, L. Fan, W. Chen, *Crit. Rev. Food Sci. Nutr.* **2022**, *62*, 1427.
[58] S. Hempel, S. J. Newberry, A. R. Maher, Z. Wang, J. N. Miles, R. Shanman, B. Johnsen, P. G. Shekelle, *JAMA, J. Am. Med. Assoc.* **2012**, *307*, 1959.
[59] C. Liu, S. M. Chen, C. X. Sun, W. C. Zuo, P. C. Wu, S. R. Wang, J. J. Dai, Y. Y. Xing, Y. L. Hou, Y. M. Ju, *Adv. Funct. Mater.* **2023**, *33*, 2300682.
[60] P. Volz, R. Brodwolf, C. Zoschke, R. Haag, M. Schäfer-Korting, U. Alexiev, *Z. Phys. Chem.* **2018**, *232*, 671.
[61] U. Alexiev, D. L. Farrens, *Biochim. Biophys. Acta, Bioenerg.* **2014**, *1837*, 694.
[62] T. Y. Kim, K. Winkler, U. Alexiev, *Photochem. Photobiol.* **2007**, *83*, 378.
[63] J. F. Swindells, C. F. Synder, R. C. Hardy, P. E. Golden, *Viscosities of Sucrose Solutions at Varoius Temperatures: Tables of Recalculated Values*, U.S. Government Printing Office, Washington, **1958**.
[64] A. Vyšniauskas, I. Lopez-Duarte, N. Duchemin, T. T. Vu, Y. Wu, E. M. Budynina, Y. A. Volkova, E. P. Cabrera, D. E. Ramirez-Ornelas, M. K. Kuimova, *Phys. Chem. Chem. Phys.* **2017**, *19*, 25252.
[65] P. Volz, A. Boreham, A. Wolf, T.-Y. Kim, J. Balke, J. Frombach, S. Hadam, Z. Afraz, F. Rancan, U. Blume-Peytavi, A. Vogt, U. Alexiev, *Int. J. Mol. Sci.* **2015**, *16*, 6960.